THE VELOCITY FIELD PARALLEL TO THE WALL IN A TURBULENT THREE-DIMENSIONAL WALL JET

Bonnie Sim
Department of Mechanical Engineering
University of New Brunswick
Fredericton, NB, Canada
Bonnie.Sim@unb.ca

Joseph W. Hall
Department of Mechanical Engineering
University of New Brunswick
Fredericton, NB, Canada
jwhall@unb.ca

ABSTRACT
The velocity field parallel to the wall of the turbulent three-dimensional wall jet was experimentally investigated through simultaneous measurements of fluctuating wall pressure and flow velocity at a Reynolds number of $Re_D = 134,000$. Particle Image Velocimetry was used to measure the lateral and streamwise flow velocities at $y/D = 0.5$ over $3 \leq x/D \leq 18$, the region where the wall jet undergoes a rapid change in lateral growth rate. The measured velocity contours showed the large lateral growth. Instantaneous velocity measurements showed significant lateral asymmetry, jet flapping, and the growth of large angled chevron structures in the jet. These structures appeared to be intermittent, change speed, and grew in size and strength with downstream development.

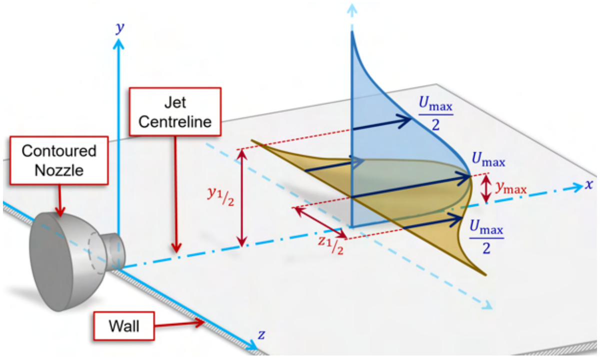

Figure 1: Schematic of the turbulent three-dimensional wall jet.

INTRODUCTION
A three-dimensional wall jet, shown in Figure 1, is a jet of fluid exiting from a finite-width opening that is directed along and develops tangentially to a surface (Launder & Rodi, 1983, 1979). Wall jets share characteristics with free jets and boundary layer flows; the outer region of the wall jet entrains ambient air into the flow similar to a free jet, while the region of flow adjacent to the wall slows due to the frictional resistance of the surface similar to a boundary layer. Wall jets are ubiquitous in industry and have a diverse range of engineering applications, primarily in heating and cooling, but also in aeronautics, ventilation, and automotives. Wall jets exhibit a comparatively large lateral growth rate in the far-field, approximately five to eight times larger than the wall-normal growth rate (Launder & Rodi, 1979; Craft & Launder, 2001), and this strong anisotropic growth rate has been the subject of extensive studies, for example (Launder & Rodi, 1979, 1983; Craft & Launder, 2001; Ewing *et al.*, 1997; Hall & Ewing, 2006, 2007*a*,*b*,*c*, 2010; Namgyal & Hall, 2013, 2016, 2021).

Although much work has been directed at studying the three-dimensional wall using velocity profiles along the jet centreline and at y_{max}, and more recently in the $y-z$ plane (Hall & Ewing, 2007*c*; Namgyal & Hall, 2016, 2021), there has never been any investigations of the three-dimensional wall jet in the x-z plane. Examination of this plane allows the continuous streamwise evolution of the lateral flow to be examined in detail. This investigation will focus on the near to intermediate field of the wall jet where the jet transitions from being dominated by near field ring structures (Ewing *et al.*, 1997; Namgyal & Hall, 2021) to the structures that causes the larger lateral growth in the jet. The present measurements will be performed in the x-z plane at $y/D = 0.5$ as this is approximately the value of y_{max} in the range examined.

EXPERIMENTAL SETUP
A schematic of the experimental facilities is shown in Figure 2. The three-dimensional wall jet exited from a contoured nozzle with an outlet diameter of $D = 38.1$ mm. The wall jet was supplied by a centrifugal blower, which was controlled by a speed regulator. In the present investigation, the experiments were conducted at an Reynolds number of $Re_D = 134,000$, corresponding to an exit velocity of $U_{\text{exit}} = 52.7 \pm 0.2$ m/s. The contoured nozzle had an area contraction ratio of 28:1 with a fifth-order polynomial contour profile, which ensured that the air exited the nozzle with a top-hat exit velocity profile. (Namgyal & Hall, 2013) showed that the mean streamwise velocity for this nozzle was uniform to 1% and the turbulence intensity was less than 0.25%.

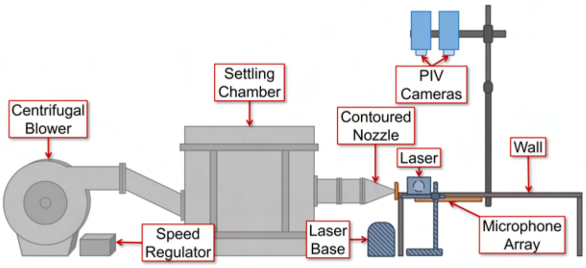

Figure 2: Schematic of the experimental facility.

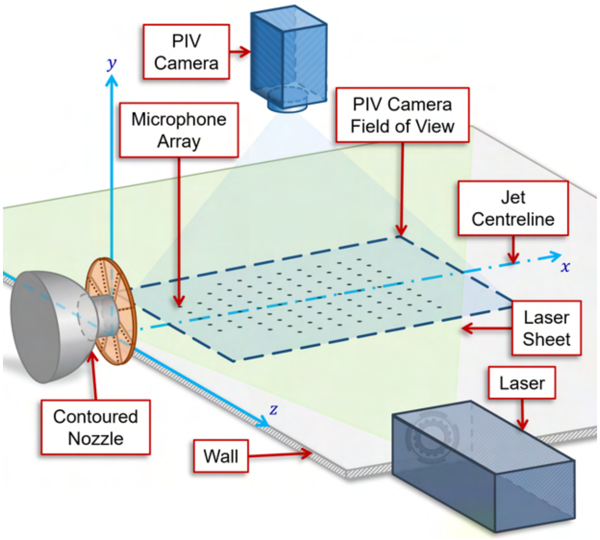

Figure 3: Current PIV configuration.

To examine the streamwise development of the structures, simultaneous measurements of fluctuating wall pressure and flow velocity were conducted in the wall jet. The flow velocity was measured using two-component Particle Image Velocimetry (PIV), in the configuration shown in Figure 2. In this study, the laser and camera were positioned as shown in Figure 3 to measure velocity on an $x-z$ plane at $y/D = 0.5$. The laser pulse separation was kept constant at 40 μs throughout the present investigation. This pulse separation allowed the PIV camera to capture the high flow velocities at the jet core, while also capturing lower velocities in the flow at the lateral extents of the jet. There were over 6000 image pairs recorded to reduced the statistical uncertainty in the data.

Prior to velocity measurements, the flow was seeded using a Rosco Model 1900 Fog Machine with clear propylene glycol fog fluid and then was intermittently reseeded to maintain a constant fog level. The tracer particle size was nominally 5 μm, which was small enough to be carried by the flow without influencing flow dynamics and jet development. (Melling, 1997) and (Tavoularis, 2005) suggested that, for particles of 5 μm, a conservative cut off frequency was 5 kHz, well above the frequency ranges focused on in this research.

Fluctuating wall pressure was measured using a two-dimensional array of 89 CUI aluminum electret condenser microphones, which had a diameter of 6 mm and a length of 5 mm. To minimize distortion and ensure uniform microphone cavities, the microphones were installed systematically flush to the underside of the wall and sensed the flow via 1.5875 mm pinholes drilled through to the top surface of the wall. The microphones were omnidirectional with a flat frequency response from 40 Hz to 20 kHz (CUI Inc, 2008), and were sampled at a rate of 50 kHz (50 302 Hz) in conjunction with the laser trigger, to reference where the PIV measurements were made.

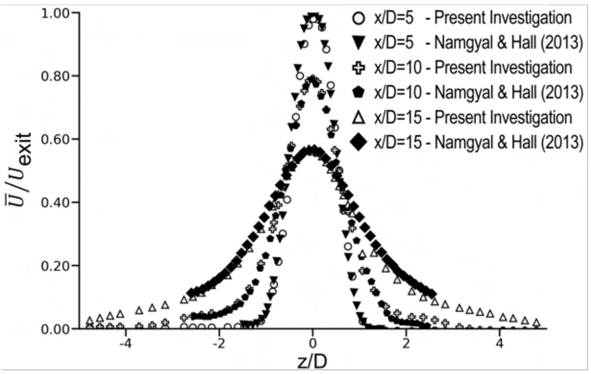

Figure 4: Profiles of the normalized mean streamwise velocities laterally across the turbulent three-dimensional wall jet.

EXPERIMENTAL RESULTS

Figure 4 shows the profiles of normalized mean ($\overline{U}/U_{\text{exit}}$) and fluctuating ($u_{\text{rms}}/U_{\text{exit}}$) streamwise velocities from the present investigation compared to profiles from the studies of (Namgyal & Hall, 2013, 2016, 2021). These profiles are plotted laterally across the jet at the height $y/D = 0.5$ at select streamwise locations ($x/D = 5$, 10, 15), and were normalized by the jet exit velocity and the nozzle diameter. The agreement between all of the profiles is quite high for the two experiments, despite Namgyal and Hall's jet having a Reynolds number ($Re_D \approx 250,000$) of almost twice that of the current experiment (Reynolds number of $Re_D = 134,000$). The agreement is all the more impressive when considering that the present PIV measurements were obtained at a single y/D position from the wall, $y/D = 0.5$, and not the true height of the maximum velocity point as is the usual modus operandi. At the streamwise extent of the PIV window, y_{max} is approximately 25% lower than the vertical position of the PIV plane (the largest deviation between the measurement plane and y_{max}). Such high agreement with the profiles at $x/D = 15$ indicates that these profiles can be used to reasonably approximate U_{max} and the lateral jet half-width.

The trend in the maximum mean streamwise velocity can be observed in the plot of the decay of the local maximum mean streamwise velocity at the centreline shown in Figure 5. The U_{max} values shown here are an approximation, not the true U_{max} values, as these measurements were performed at a single y/D value. The measurements from the present investigation were plotted against the data from the previous studies of (Namgyal & Hall, 2013, 2016, 2021; Hall & Ewing, 2007*b*,*a*, 2010; Sun, 2002; Sun & Ewing, 2002), which are all taken at y_{max}. The velocities have either been normalized by U_{exit} or the pipe mean velocity, U_0, depending on the nozzle exit shape. The decay in normalized maximum streamwise velocity has been plotted from the present investigation for discrete streamwise positions for comparison with previous studies.

The turbulent three-dimensional wall jet was characterized through contours of mean and fluctuating streamwise and lat-

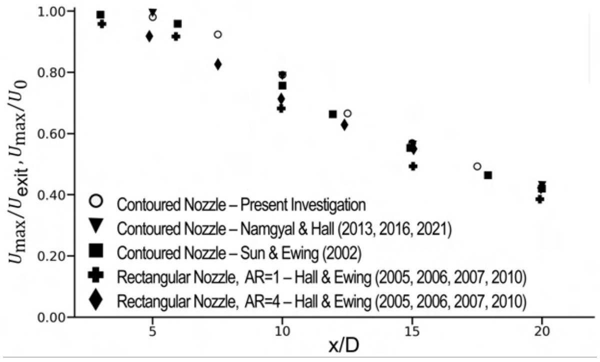

Figure 5: The decay of the local maximum streamwise velocity of the turbulent three-dimensional wall jet.

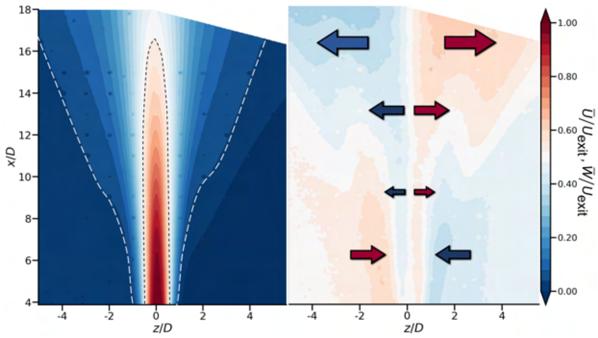

Figure 6: Contours of the normalized mean streamwise and lateral velocities at $y/D = 0.5$.

eral velocities measured with PIV. The contours of the mean velocities and the RMS fluctuating velocities, normalized by U_{exit}= 52.7m/s, are depicted in Figure 6. The left plot of Figure 6 shows the contours of the normalized mean streamwise velocity, $\overline{U}/U_{\text{exit}}$, and the right plot shows the contours of the normalized mean lateral velocity, $\overline{W}/U_{\text{exit}}$. The lateral and streamwise coordinates were normalized by the nozzle diameter, $D = 38.1$ mm. The points observed on the PIV images are the microphone pinholes and did not affect the observations of the flow field.

The normalized mean streamwise velocities $\overline{U}/U_{\text{exit}}$ (Figure 6) showed a region of fast moving air in the core of the wall jet, consistent with previous jet literature (Craft & Launder, 2001; Launder & Rodi, 1979, 1983; Namgyal & Hall, 2013). The potential core was present at $x/D \leq 6$; the potential core is characterized by a region of fluid with a mean streamwise velocity marginally less than the exit velocity while exhibiting low turbulence. The presence of the potential core can be clearly observed at this location in the turbulent velocity contours as the low turbulence region at the jet centre bracketed by the high turbulence of the shear-layers. From the turbulent contours, the potential core can be seen to persist to $x/D \approx 7$ in this jet, consistent with the contoured nozzle wall jet literature (Namgyal & Hall, 2013, 2016, 2021). The maximum streamwise velocity decreased rapidly downstream of the potential core collapse, and, by $x/D = 10$, the mean streamwise velocity at the centre of the jet was $\sim 75\%$ of the exit velocity. By $x/D = 18$, this the maximum streamwise velocity was less than 50% of the exit velocity.

The contours of mean lateral velocity, $\overline{W}$, in Figure 6 also clearly show the large lateral growth in the wall jet after the collapse of the potential core. The jet grew slowly until $x/D \approx 10$, after which it rapidly widened. This large lateral growth was accompanied by a corresponding increase in the magnitude of the outwardly directed mean lateral velocity on either side of the jet centreline. Interestingly, the magnitude of the mean lateral velocity continued to increase and was still growing stronger at $x/D = 18$ (the streamwise extent of the PIV window). This indicates that the wall jet had not reached the far-field by $x/D = 18$, consistent with the literature that the turbulent three-dimensional wall jet develops more slowly than other turbulent jet flows (Sun, 2002; Sun & Ewing, 2002). It is possible that the wall jet approaches self-similarity more slowly than other jet flows because of the time it takes for the establishment of these lateral velocities, which have not plateaued and started to decrease, as is expected in the far-field.

Figures 7 through 10 show the normalized instantaneous streamwise and lateral velocities and fluctuating velocities for turbulent three-dimensional wall jet for four independent instants (or snapshots). Figure 7 shows the normalized instantaneous streamwise velocity, U_i/U_{exit}, for the four independent instants and Figure 8 shows the corresponding instantaneous lateral velocity, W_i/U_{exit}, for the same independent instants. Figures 9 and 10 show the associated normalized instantaneous fluctuating streamwise and lateral velocities, respectively, for the same four independent instants.

From initial observations of the instants, it is apparent that the turbulent three-dimensional wall jet displays significant variation from instant to instant. The contours of instantaneous U_i/U_{exit} shown in Figure 7 show clear asymmetry in the development of the turbulent three-dimensional wall jet. The instants of U_i/U_{exit} show a flow-field that typically exhibits asymmetry in the jet core, as indicated by the quasi-periodic waviness at the edges of the jet core (particularly evident in snapshot n_3, over the region denoted A). The jet also shows lateral deviation, almost a flapping, from the centreline downstream of the collapse of the jet core, especially in snapshots n_1, n_2, and n_4, denoted by B, C, and D, respectively. Additionally, there are also higher-moving streamwise velocity regions that break away from the jet core and convect downstream. These regions of instantaneous faster moving streamwise velocity, U_i/U_{exit}, are particularly evident in n_1 and n_4, and are denoted by E and F.

The contours of W_i/U_{exit} shown in Figure 8 are the corresponding lateral component of the velocity for the snapshots shown in Figure 7. Despite the complexity of the flow, there are features consistently evident in the instantaneous contours, W_i/U_{exit}, that were noted in the contours of mean lateral velocity, $\overline{W}/U_{\text{exit}}$: upstream of the collapse of the potential core, the instantaneous lateral flow was directed towards the jet centreline from the ambient surrounding air, as indicated by the inward-pointing arrows upstream of $x/D \approx 10$ on Figure 8. Downstream of the point where the core of the jet collapses, there are large regions of lateral flow directed outwards. These regions contribute to the lateral growth of the wall jet and are denoted by the outward-pointing arrows downstream of $x/D \approx 10$. These large regions of lateral flow are particularly evident in instants n_1 (G), n_2 (H), and n_4 (I-K).

Additionally, there appears to be some regions of alternating positive and negative instantaneous lateral flow, which is indicative of the passage of organized structures. These alternating regions of lateral flow also seem to correspond to flapping in the jet and asymmetric lateral deviations of the jet as observed in the contours of instantaneous streamwise velocity. The flapping is particularly evident in instant n_4, where large organized regions of lateral flow (denoted I, J, and K) cause alternating lateral deviations of the mean streamwise flow (identified previously by D). The flapping of the jet is also observed in instant n_2, as the lateral deviation of the streamwise flow, labelled C. The corresponding contours of W_i/U_{exit} exhibit strong, and oppositely directed, lateral flow, denoted as H. When flapping is not observed in the jet, like instant n_3, the contours of instantaneous lateral velocity do not exhibit these large organized regions of W_i/U_{exit}. Therefore, flapping of the jet is associated with the passage of strong, alternating, instantaneous lateral flow.

Figures 9 and 10 show the normalized instantaneous fluctuating streamwise u_i/U_{exit} and lateral velocities w_i/U_{exit}, respectively, for the same snapshots shown in Figures 7 and 8. Instantaneously, there is significant variation in the contours of fluctuating velocity. However, the passage of large regions of organization is evident. The streamwise fluctuations have large organized regions that are elongated in the streamwise direction, while the contours of lateral fluctuations are spatially oriented with long axis perpendicular to the flow direction, as expected. In general, these regions are nominally $\sim 2D$ in the near-field but do grow slightly to $3 \sim 4D$ in length. These lengths correspond to the integral length scales estimated from the autocorrelations and RMS fluctuating streamwise velocities at $(x/D, z/D) = (5, 0)$, approximately $1.7 \sim 2.3D$, and $(x/D, z/D) = (15, 0)$, approximately $3 \sim 3.7D$. The elongation of the coherent streamwise fluctuations is particularly evident in n_1 (L), n_2 (M and N), and n_4 (O, P, and Q). The elongation of the lateral fluctuations is primarily evident in n_2 (R). These elongated adjacent regions of strong positive and negative fluctuations in u_i/U_{exit} are likely indicative of the passage of a vortical structure, especially when there are analogous regions of strong alternating positive and negative lateral fluctuations in the streamwise direction at the same spatial position. For instance, n_2 exhibits elongated streamwise fluctuations at M, where there are laterally stretched lateral fluctuations, denoted by R. These adjacent regions could be indicative of rotation in the flow field and the passage of vortical structures downstream. Furthermore, as is evident through the elongated streamwise and stretched lateral fluctuations in n_4, denoted and directed by the arrows at O, P, and Q, that stronger and more organized u_i/U_{exit} and w_i/U_{exit} fluctuations are associated with flapping in the wall jet. The structures are surprisingly long, $\sim 4D$ at $x/D \approx 14$ onwards, as indicated by the coherence in the u_i/U_{exit} contours, which is very unlike the model of a vortex ring, which would be expected to be short in the streamwise direction. The ring model suggests structures on the scale of the nozzle (Namgyal & Hall, 2021), while the scale of the organized streamwise fluctuations is significantly longer, as shown on n_2 (M and N) and n_4 (O, P, and Q).

To examine the organization in the flow, the pressure-velocity correlations, $\langle up_i \rangle$ and $\langle wp_i \rangle$, were computed using the synchronized measurements of fluctuating wall pressure and fluctuating velocity; an example of the synchronized fluctuating wall pressure and fluctuating velocity is shown in Figure 11. George *et al.* (1984) showed that pressure spectra roll off much more quickly than the velocity field, therefore, the unsteady wall pressure field represents a low-pass filtered velocity field; the steeper roll off in the pressure spectra indicating the higher frequencies and passage of smaller structures are not evident in the wall pressure field. The pressure-velocity correlations were calculated with the fluctuating wall pressure measured

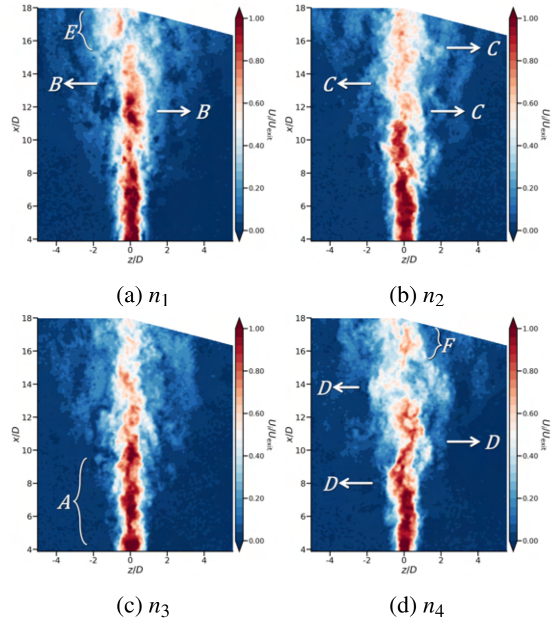

(a) n_1 (b) n_2

(c) n_3 (d) n_4

Figure 7: Contours of normalized instantaneous streamwise velocities, U_i/U_{exit}, at $y/D = 0.5$.

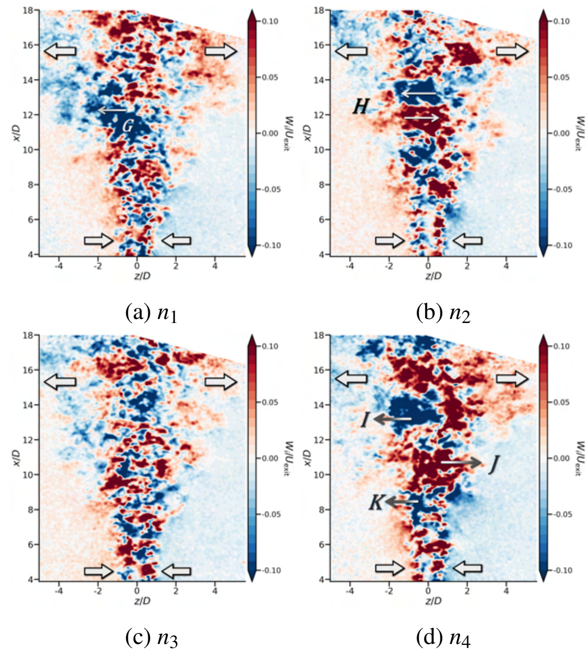

(a) n_1 (b) n_2

(c) n_3 (d) n_4

Figure 8: Contours of normalized instantaneous lateral velocities, W_i/U_{exit}, at $y/D = 0.5$.

with each microphone p_i and the fluctuating streamwise and lateral velocity measured at the PIV-plane $y/D = 0.5$.

The normalized streamwise pressure-velocity correlations, $\langle p_i u \rangle / (\sigma_{p_i} \sigma_u)$, are shown in Figure 12 for the microphones in the streamwise rows at $x/D = 5$, 10, and 15 and the lateral positions $z/D = -1$, 0, and 1; the microphone location is identified with an $\times$ symbol.The level of correlation provides insight into how the passage of pressure fluctuations at the wall is linked to organized turbulent motion in the parallel plane at $y/D = 0.5$.

At $x/D = 5$, the streamwise pressure-velocity correlations

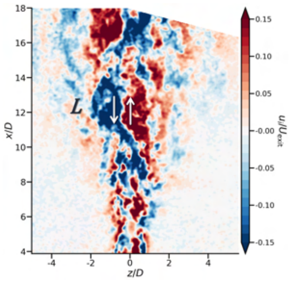

(a) n_1

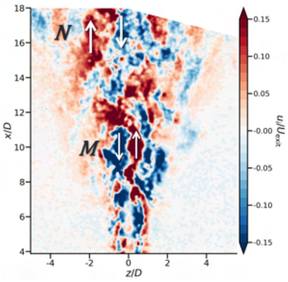

(b) n_2

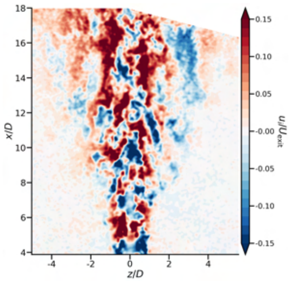

(c) n_3

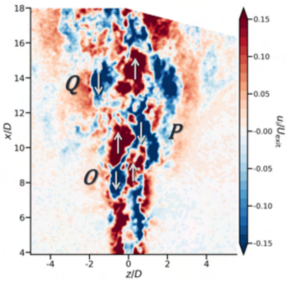

(d) n_4

Figure 9: Contours of normalized instantaneous fluctuating streamwise velocities at $y/D = 0.5$.

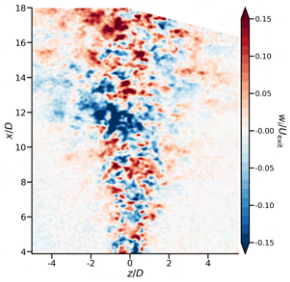

(a) n_1

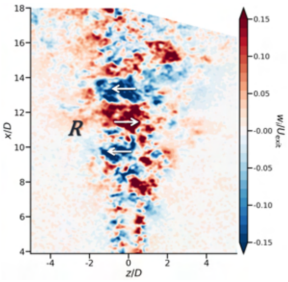

(b) n_2

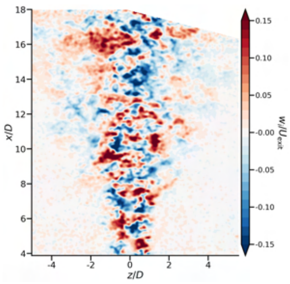

(c) n_3

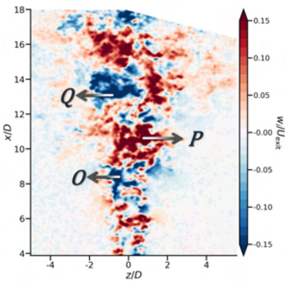

(d) n_4

Figure 10: Contours of normalized instantaneous fluctuating lateral velocities at $y/D = 0.5$.

$\langle p_i u\rangle/(\sigma_{p_i}\sigma_u)$ consist of alternating regions of positive and negative correlations. The regions of correlation are spatially smaller than those further downstream, and do not persist for very large distances from the microphone at the centreline, compared to the correlations at $z/D = \pm 1$. The correlations at $z/D = \pm 1$ appear to be mirrored about the centreline. At $x/D = 5$ the regions of positive and negative correlations appear to be more separated than those downstream, but developing angled chevron structures can be observed in these pressure-velocity correlations, and are identified by the dashed lines on Figure 12. For instance, the pressure-velocity

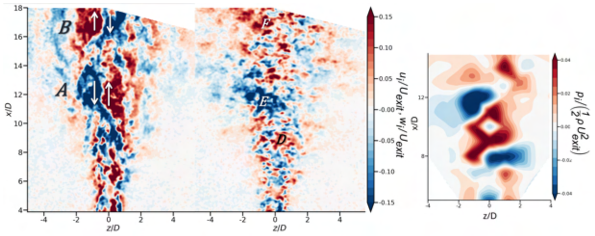

Figure 11: Contours of synchronized fluctuating streamwise and lateral velocities at $y/D = 0.5$ and fluctuating wall pressure.

correlations with the microphone at $(x/D, z/D) = (5, -1)$ exhibit a positive correlation at $(x/D, z/D) = (5, 0)$ is partially connected to regions of correlation at $(x/D, z/D) = (4, -1)$; the correlation with the microphone at $(x/D, z/D) = (5, 1)$ exhibits an analogous correlation configuration but mirrored about the centreline. At $x/D = 5$, these angled structures do not appear to be fully developed closer to the nozzle, as shown by the spatially discrete regions of correlation at $z/D = \pm 1$. However, the length of each leg of the chevron is approximately $1 \sim 2D$, with the leg of the chevron closest to the centreline being nominally shorter than the outward leg. The symmetry of the chevron remains relatively consistent with downstream development over the measurement region Additionally, the angle between the legs/pins of the chevron hairpin was estimated to be $\sim 55°$.

At $(x/D, z/D) = (10, \pm 1)$, the pressure-velocity correlations have grown to encompass a larger spatial region and persist further downstream; the chevron legs are approximately $\sim 3D$ in length. By $x/D = 15$, the pressure-velocity correlations with the microphones off of the centreline have further grown ($3 \sim 4D$ in length), encompassing a larger region upstream and downstream of the microphone. Similar to the pressure-velocity correlations at $x/D = 5$, the correlations at $z/D = 1$ appear to approximately mirror those at $z/D = -1$ for the microphones at $x/D = 10$ and 15. The angling in the organization that was developing at $x/D = 5$ is more evident in the correlations at $(x/D, z/D) = (10, \pm 1)$ and even more so in the correlations at $(x/D, z/D) = (15, \pm 1)$. With downstream development, as evident at $x/D = 10$ and $x/D = 15$, this angled chevron region of positive $\langle p_i u\rangle/(\sigma_{p_i}\sigma_u)$ grows and becomes more distinct, which suggests that the structures off of the centreline are likely larger in size and/or persist further downstream. The angle in these hairpin chevron structures appears to increase with downstream development, from approximately $\sim 55°$ at $x/D = 5$ to $\sim 60°$ at $x/D = 15$. Since the legs of the chevron in the correlation extend further upstream at $x/D = 15$ than at $x/D = 10$, it indicates that the structures in the flow are growing with downstream development. The nominal length grows from $1.5 \sim 2D$, consistent with the length in the instantaneous snapshots (Figures 9 and 10), to $3 \sim 4D$. Using two-point velocity correlations, (Sun, 2002) argued that the lateral legs of the structure tilt outward as the structure evolves downstream. This is consistent with the pressure-velocity correlations.

The regions of correlation are larger for the microphones off of the centreline than on the centreline, which is evident in the correlations at $z/D = \pm 1$ compared to those at $z/D = 0$. At the centreline, the regions of strong positive and strong negative $\langle p_i u\rangle/(\sigma_{p_i}\sigma_u)$ correlations are weaker, spatially smaller, and appear to decay rapidly with downstream development. Since

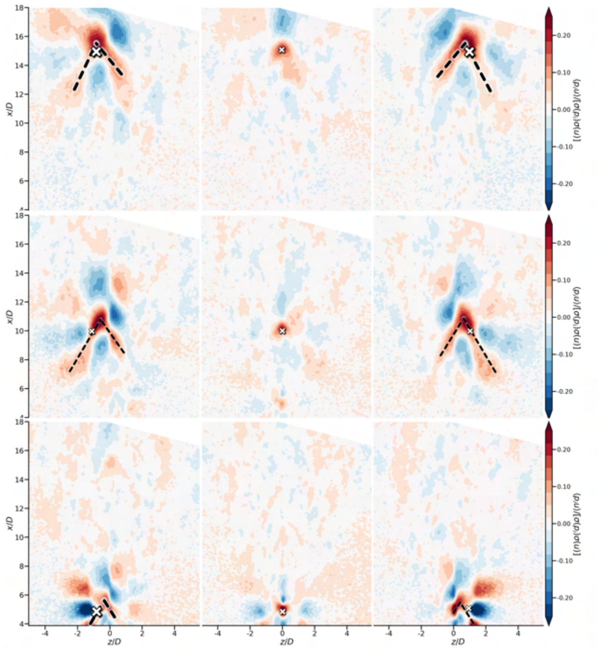

Figure 12: Contours of the normalized streamwise pressure-velocity correlations, $\langle p_i u\rangle/(\sigma_{p_i}\sigma_u)$, for the specified microphones at $y/D = 0.5$.

these correlation regions do not persist very far downstream, it suggests that at the centreline there are smaller structures than off the centreline, which are evolving more rapidly with downstream convection, which is consistent with the findings of (Hall & Ewing, 2010) in their spectral LSE. Compared to the size and strength of the correlations at the centreline, the at $z/D = \pm 1$ are much larger, stronger, and persist further upstream and downstream of the correlated microphone. This suggests that the structures off of the centreline are more organized, which is consistent with the trends seen in the analysis of the fluctuating wall pressure.

CONCLUSIONS

Simultaneous PIV and unsteady wall pressure measurements were performed in the near and intermediate field of a turbulent three-dimensional wall jet. The mean measurements are in good agreeenment with results from the literature and contours show strong regions of inward lateral entrainment prior to the collapse of the potential core. Beyond the collapse of the potential core, the lateral velocity contours were much wider and oriented to drive the flow laterally outward.

Instantaneously, the snapshots of streamwise and lateral velocities velocities show a highly variable asymmetric flow field and a pronouced flapping behvaiour downstream of the collapse of the potential core in the jet. The flapping is associated with strong coherent alternating lateral velocity fluctuations, consistent with the passage of coherent structures.

Pressure-velcocity correlations were computed to better examine the coherent structures in the flow. The results revealed the presence of chevron shaped structures that were much larger on either side of the jet centreline and away from the centreline of the jet. These structures grew longer as the evolved downstream and became more angled to the jet centreline; both of these traits serve to enhance the lateral growth of this flow.

References

Craft, T. J. & Launder, B. E. 2001 On the spreading mechanism of the three-dimensional turbulent wall jet. *J. Fluid Mech.* **435**, 305–326.

CUI Inc 2008 Electret condensor microphone. Data Sheet Part. No. CMC-5044PF-A. CUI Inc.

Ewing, D., Benaissa, A., Pollard, A., Citriniti, J., Abrahamsson, H. & Lofdahl, L. 1997 Contribution of large structures to the anisotropic spread rate in a wall jet issuing from a round nozzle. In *Tenth Int. Symp. Transp. Phenom. Therm. Sci. Process Eng.*.

George, W. K., Beuther, P. D. & Arndt, R. E. A. 1984 Pressure spectra in turbulent free shear flows. *J. Fluid Mech.* **148**, 155–191.

Hall, J. W. & Ewing, D. 2006 A combined spatial and temporal decomposition of the coherent structures in the three-dimensional wall jet. In *44th AIAA Aerospace Sciences Meeting and Exhibit*. Reno, NV USA.

Hall, J. W. & Ewing, D. 2007*a* The asymmetry of the large-scale structures in turbulent three-dimensional wall jets exiting long rectangular channels. *J. Fluids Eng.* **129** (7), 929–941.

Hall, J. W. & Ewing, D. 2007*b* Spectral linear stochastic estimation of the turbulent velocity in a square three-dimensional wall jet. In *Proc. ASME/JSME 2007 5th Joint Fluids Eng. Conf.*, pp. 1013–1023. San Diego, CA USA.

Hall, J. W. & Ewing, D. 2007*c* Three-dimensional turbulent wall jets issuing from moderate-aspect-ratio rectangular channels. *AIAA J.* **45** (6), 1177–1186.

Hall, J. W. & Ewing, D. 2010 Spectral linear stochastic estimation of the turbulent velocity in a square three-dimensional wall jet. *J. Fluids Eng.* **132** (5), 051203.

Launder, B. E. & Rodi, W. 1979 The turbulent wall jet. *Prog. Aerosp. Sci.* **19**, 81 – 128.

Launder, B. E. & Rodi, W. 1983 The turbulent wall jet measurements and modeling. *Ann. Rev. Fluid Mech.* **15** (1), 429–459.

Melling, A. 1997 Tracer particles and seeding for particle image velocimetry. *Meas. Sci. Tech.* **8** (12), 1406–1416.

Namgyal, L. & Hall, J. W. 2013 Coherent streamwise vortex structures in the near-field of a the three-dimensional wall jet. *J. Fluids Eng.* **135** (6).

Namgyal, L. & Hall, J. W. 2016 Reynolds stress distribution and turbulence generated secondary flow in the turbulent three-dimensional wall jet. *J. Fluid Mech.* **800**, 613–644.

Namgyal, L. & Hall, J. W. 2021 Coherent streamwise vortex structure of a three-dimensional wall jet. *Fluids* **6** (1), 35.

Sun, H. 2002 Development of three-dimensional turbulent wall jets. PhD thesis, McMaster University, Hamilton, Ontario, Canada.

Sun, H. & Ewing, D. 2002 The development of three-dimensional wall jet. In *Proc. 48th Ann. Conf. Canadian Aeronautics and Space Institute*. Toronto, Canada.

Tavoularis, S. 2005 *Measurement in Fluid Mechanics*. Cambridge; New York: Cambridge University Press.